Thin Solid Films 519 (2011) 7959–7965

Contents lists available at ScienceDirect

Thin Solid Films

journal homepage: www.elsevier.com/locate/tsf

Structural and optoelectronic properties of Al-doped zinc oxide films deposited on flexible substrates by radio frequency magnetron sputtering

C.H. Tseng [a], C.H. Huang [b], H.C. Chang [b], D.Y. Chen [c], C.P. Chou [a], C.Y. Hsu [b,*]

[a] Department of Mechanical Engineering, National Chiao Tung University, Taiwan, ROC
[b] Department of Mechanical Engineering, Lunghwa University of Science and Technology, Taiwan, ROC
[c] Department of Mechanical Engineering, Hwa Hsia Institute of Technology, Taiwan, ROC

ARTICLE INFO

Article history:
Received 5 May 2010
Received in revised form 29 April 2011
Accepted 10 May 2011
Available online 18 May 2011

Keywords:
Zinc oxide
Transparent conducting film
Buffer layer
Carrier concentration

ABSTRACT

Al-doped zinc oxide (AZO) thin films were deposited onto flexible polyethylene terephthalate substrates, using the radio frequency (RF) magnetron sputtering process, with an AZO ceramic target (The Al_2O_3 content was about 2 wt.%). The effects of the argon sputtering pressure (in the range from 0.66 to 2.0 Pa), thickness of the Al buffer layer (thickness of 2, 5, and 10 nm) and annealing in a vacuum (6.6×10^{-4} Pa), for 30 min at 120 °C, on the morphology and optoelectronic performances of AZO films were investigated. The resistivity was 9.22×10^{-3} Ω cm, carrier concentration was 4.64×10^{21} cm^{-3}, Hall mobility was 2.68 cm^2/V s and visible range transmittance was about 80%, at an argon sputtering pressure of 2.0 Pa and an RF power of 100 W. Using an Al buffer decreases the resistivity and optical transmittance of the AZO films. The crystalline and microstructure characteristics of the AZO films are improved by annealing.

1. Introduction

Transparent conducting oxide (TCO) films are currently of great commercial and scientific importance for applications such as light-emitting diodes, amorphous silicon solar cells, gas sensors, surface acoustic wave devices and other optoelectronic devices [1]. Materials such as indium tin oxide (ITO), tin oxide (SnO_2) and zinc oxide (ZnO) films are well-known, typical transparent conductive films [2]. The advantages of ZnO are its material cost, non-toxicity, high crystallinity and stability in hydrogen plasma processes, compared with ITO, In_2O_3 and SnO_2 films, so ZnO is an attractive material for use as a TCO [3].

Non-doped ZnO usually has high resistivity, due to low carrier concentration. Among the various dopants available, for n-type ZnO thin films, Group III metals, such as Al, In and Ga have been found to be the most suitable materials. These elements are known to enhance the electrical and optical properties of the ZnO film [4]. The ZnO films doped with these impurities, Al-doped ZnO films demonstrate a wider band gap, higher visible transmittance and lower resistivity, as compared to ITO and SnO_2[5].

Transparent conducting films deposited on polymer substrates have many merits, compared with those deposited on a conventional glass substrate. They are lighter, smaller, have greater impact resistance, ease of transport and flexibility [6]. However, polymer substrates have some disadvantages, such as lower thermal resistance, weaker mechanical strength and a higher coefficient of thermal expansion, as compared to glass substrates [7]. Deposition of TCO films on polymer substrates presents a significant problem, because the substrate temperature needs to be relatively low [8].

This paper considers the deposition of high quality ZnO:Al (98:2 wt.%) transparent conductive thin films on polyethylene terephthalate (PET) substrates, using radio frequency (RF) magnetron sputtering at room temperature. The electrical characteristics (Hall effect and resistivity as a function of argon sputtering pressure), optical transmittance, structure (X-ray diffraction (XRD) and transmission electron microscopy (TEM)) and surface morphology (SEM, JEOL, JSM-6500F) were examined.

2. Experimental procedure

The Al-doped zinc oxide (AZO) transparent conducting films and Al buffer layer were prepared on PET substrates, using an RF (13.56 MHz) magnetron sputtering process, with a base pressure of 6.6×10^{-4} Pa. PET substrate is a low-cost, flexible polymer, displaying excellent optical and mechanical properties. The characteristics of PET substrates are summarized in Table 1.

The ceramic targets, with a mixture of ZnO powder (99.99% purity) and Al_2O_3 powder (99.99% purity), were commercially available, hot-pressed and sintered targets (Elecmat, USA). The amounts of Al_2O_3 dopant in the ZnO powder ranged from 2 to 5% [9,10]. We chose Al_2O_3 at about 2 wt.%, for this study. Prior to the experiments, the PET substrates were ultrasonically cleaned, using acetone, methanol and deionized water, and then dried by blowing with nitrogen. Before deposition, the targets were pre-sputtered, for 5 min, to remove any

* Corresponding author. Fax: +886 2 82094845.
E-mail address: cyhsu@mail.lhu.edu.tw (C.Y. Hsu).

0040-6090/$ – see front matter © 2011 Elsevier B.V. All rights reserved.
doi:10.1016/j.tsf.2011.05.017

Table 1
Characteristics of the PET substrate.

Substrate thickness (mm)	0.25
Specific gravity (g/cm^3)	1.30
Water absorption (%)	0.3
Refractive index	1.40
Thermal expansion coefficient (cm/cm °C)	5–8×10^{-5}
Retardation (nm)	68
Transmittance (at 550 nm)	83
Glass transition temperature (°C)	70

contamination. Table 2 lists the experimental conditions for the AZO film and Al buffer layer.

The structural properties and crystallite size were investigated using XRD (Rigaku-2000 X-ray Generator). The Cu Kα radiation (40 kV, 30 mA and λ = 0.1541 nm) had a grazing incidence angle of 1° and the scanning rate was 5°/min. The surface morphologies were analyzed using field emission scanning electron microscopy (SEM, JEOL, JSM-6500F), the operating voltage is 10 kV. The sheet resistance was measured using the four-point probe method (Mitsubishi chemical MCP-T600). The carrier concentration and Hall mobility were measured by the Van der Pauw method. Hall effect was measured (Nanometrics/Accent /NAN-HL5500PC) at room temperature. Optical transmittance was measured in the range of 300–800 nm, using an UV/Visible/NIR spectrophotometer (Hitachi, U-4100).

3. Results and discussion

The AZO thin films deposited on polymeric substrates showed very good adherence. No crack or peel-off of the films was observed, after deposition. Fig. 1(a) shows the schematic diagram for the pull-off adhesion test between the substrate and the AZO thin film, which is similar to an engineering tensile strength test [11,12]. In this study, the direct tensile test method, rather than interfacial shear through bending, or lap-shear, was used to measure the adhesion strength. The tensile test method measures thin film adhesion strength precisely, in a way that corresponds with cross cut test results.

A steel bar, of 5 mm diameter, was used for the test. Adhesive epoxy (3M Scotch-Weld, Epoxy adhesives DP-460) was applied between the steel bar and the AZO thin film. Fig. 1(b) shows the photograph of AZO films (zone 1), which was the original peel-test zone, and zone 2, a circular region which shows the fractured surface, after mechanical testing of the AZO film.

Table 3 shows the adhesion strength of AZO films, as measured by a pull test, with and without Al buffer layers. The pulling test was done at room temperature and atmospheric pressure, using a motor crosshead speed of 1 mm/min. Tests were repeated twice, for each

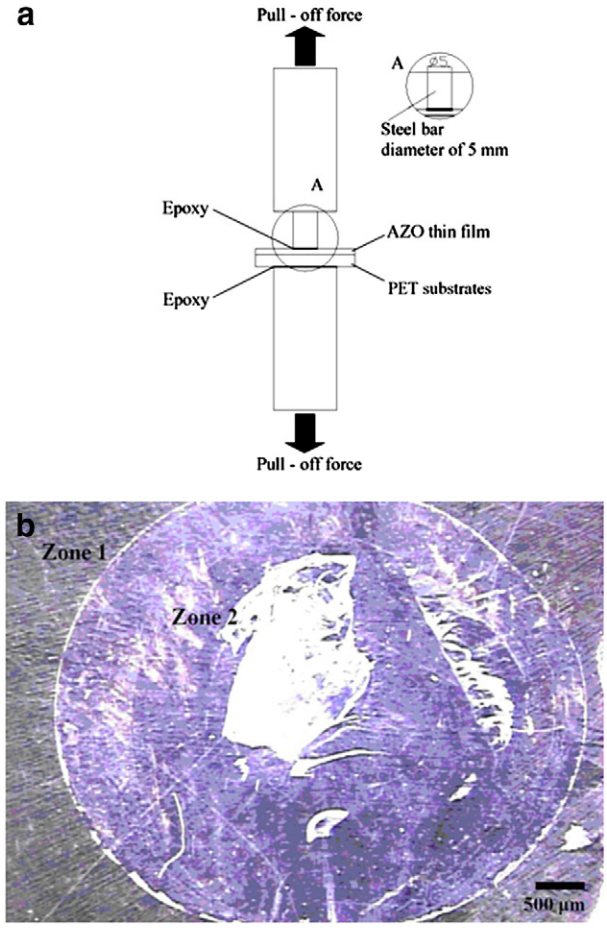

Fig. 1. (a) Schematic diagram of pull-off adhesion test, (b) Photograph of AZO films (zone 1) and fracture surface (zone 2), after mechanical test (50×).

sample. For AZO films deposited on PET substrates, with and without an Al buffer layer, the peel off stresses were 24.35 and 17.31 MPa, respectively. This demonstrates that the Al buffer layer increases the adhesive strength of the AZO thin films.

Fig. 2 shows the deposition rates of AZO/PET films, as a function of sputtering pressure (deposition parameters of AZO films are listed in Table 2). Clearly, the deposition rate reaches its maximum value of 6.31 nm/min at a sputtering pressure of 1.0 Pa and then decreases, as sputtering pressure increases further. This result is similar to those recorded by Ma et al. [13] and Lee et al. [14].

Fig. 3 (a) shows the XRD patterns for AZO films grown on PET substrates (the film thickness was 200 nm), as a function of sputter pressure. All films display (002) peaks, indicating that the AZO films have a hexagonal ZnO Wurtzite structure, with a marked orientation along the c-axis, perpendicular to the substrate surface. Fig. 3(b) shows the (002) peak positions and the full width at half maximum value (FWHM) for the AZO films' XRD pattern, as a function of sputter pressure. This reveals that the diffraction peak position, 2θ, shifts from

Table 2
Experimental conditions for AZO and Al buffer layer.

	AZO	Al buffer layer
Substrate	PET or Al/PET	PET
Target	ZnO:Al_2O_3 (98:2 wt.%);99.995% purity	Al;99.99% purity
Substrate dimension	20 mm×20 mm×0.25 mm	
Target size	51.2 mm diameter	
Gas	Argon (99.995%)	
Base pressure	6.6×10^{-4} Pa	
Substrate rotate vertical axis	20 rpm	
Substrate-to-target distance	100 mm	
Substrate temperature	Room temperature	
Sputtering pressure (Pa)	0.66, 1.0, 1.33, 2.0	1.0
Thickness (nm)	200	2, 5,10
RF power (W)	100	50
Deposition rate (nm/min)	5.48, 6.31, 5.93, 5.86	3.96

Table 3
Adhesive strength of AZO films, measured by pull test, with and without Al buffer layers.

	Maximum loading (kgf)	Maximum loading displacement (mm)	Peel off stress (MPa)
AZO/Al/PET	14.9	0.133	24.35
AZO no buffer layer	10.59	0.15	17.31

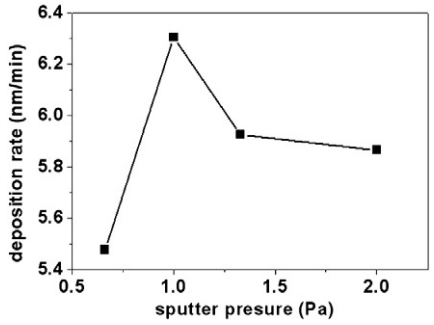

Fig. 2. The effect of sputtering pressure on the deposition rate of AZO/PET films.

34.40°, at a 1.0 Pa sputter pressure, to a higher angle of 34.50°, at a sputter pressure of 2.0 Pa.

To assess the crystalline quality of the AZO films, the FWHM values of (002) peak and the crystallite dimensions estimated were used in conjunction with Scherrer's formula [15]. As the sputter pressure changes from 0.66 to 1.0 Pa, the FWHM of the films increases, initially, and then decreases to a minimum value of 0.352, at a sputter pressure of 2.0 Pa. The calculated grain sizes of the AZO films are presented in Fig. 3(c). It can be seen that the grain size decreases from 21.34 to 20.07 nm, when the sputter pressure is increased from 0.66 to 1.0 Pa. Grain size then increases to 23.62 nm, when the sputter pressure is further increased to 2.0 Pa. These results are consistent with the SEM micrographs for AZO films, shown in Fig. 4.

Fig. 5 shows the electrical resistivity, carrier concentration, and Hall mobility for the AZO grown on PET substrates, as a function of sputter pressure. The carrier concentration of the AZO films ranges from 6.59×10^{20} cm^{-3}, at 0.66 Pa, to 4.64×10^{21} cm^{-3}, at 2.0 Pa. The minimum values for Hall mobility and resistivity were 2.68 cm^2/V s and 9.22 mΩ cm, respectively, for the film deposited at 2.0 Pa. The experimental results show increased carrier concentration, and a decrease in Hall mobility [13] and electrical resistivity for AZO/PET films, as sputtering pressure is increased. Similar behavior was noted by Jang et al. [16].

The optical transmittance spectra for the AZO/PET thin film, between wavelengths 300 and 800 nm, are shown in Fig. 6. The thickness is around 200 nm, for all films. For the purpose of comparison, the spectrum for the PET substrate (solid line) is also presented. The average optical transmittance of all the films is over 78%, including those using the PET substrate.

The crystalline quality and structure of the films were improved by applying the buffer layers [17]. In this study, the Al thin films were grown on PET substrates, at room temperature, to serve as buffer layers. The RF power was 50 W, the deposition rate was 3.96 nm/min and the thicknesses of the Al buffers were 2, 5, and 10 nm, respectively (deposition parameters of the Al buffer layer are listed in Table 2).

Fig. 7 shows the SEM micrographs for AZO deposited on Al buffer layers of different thicknesses (2, 5, and 10 nm, respectively). It can be seen that an increase in the Al buffer layer thickness, causes an improvement in the crystalline quality of the AZO films and the grain sizes become larger and more uniformly distributed. An increase in crystallite size causes an increase in carrier concentration, which is related to grain scattering [18,19].

XRD measurements were performed, to confirm the crystalline quality of the deposited AZO/Al/PET thin films. Fig. 8 shows the XRD spectra of (a) Al/PET buffer and (b) AZO/Al/PET. For Al buffer thicknesses of 10 nm, the peak intensity ($2\theta = 39.41°$ for (200) plane of Al and $2\theta = 34.39°$ for (002) plane of AZO) yields the largest and the smallest FWHM values.

Fig. 9(a) shows the electrical resistivity of AZO thin films grown on Al/PET, as a function of Al buffer thickness, using AZO films with a

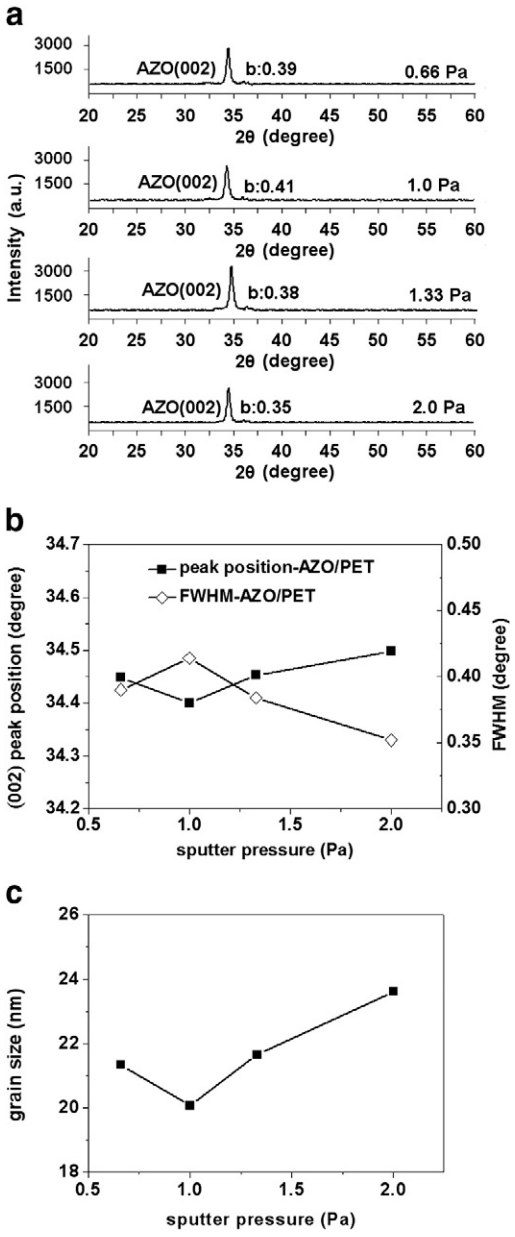

Fig. 3. (a) X-ray diffraction patterns, (b) variation in peak position and FWHM of the (002) peak, and (c) grain size, at different sputtering pressures, for 200 nm thick AZO films deposited on PET substrates.

thickness of 200 nm, deposited at a sputter pressure of 2.0 Pa. It is clear that as the Al buffer layer increases, from no buffer to 10 nm thickness, the resistivity gradually decreases, from 9.22 mΩ cm to as low as 2.6 mΩ cm. The deposition process for AZO/Al/PET causes a decrease in resistance, because the buffer layer between the film and the substrate improves the crystalline quality of the film [20]. It is also possible that, since the Al has a high diffusion coefficient, it can migrate quickly into the AZO film, during the deposition process [21]. The presence of an Al buffer increases the carrier concentration and reduces the resistance of the film.

It is well known that post-annealing is important to the improvement of crystal quality. During the annealing process, dislocations and other defects occur in the material and there is adsorption/decomposition. Fig. 9(b) shows the electrical resistivity of AZO/Al/PET thin films, annealed in a vacuum (6.6×10^{-4} Pa) at temperatures of 120 °C, for a period of 30 min. It can be seen that annealing treatment decreases the resistivity of AZO thin films.

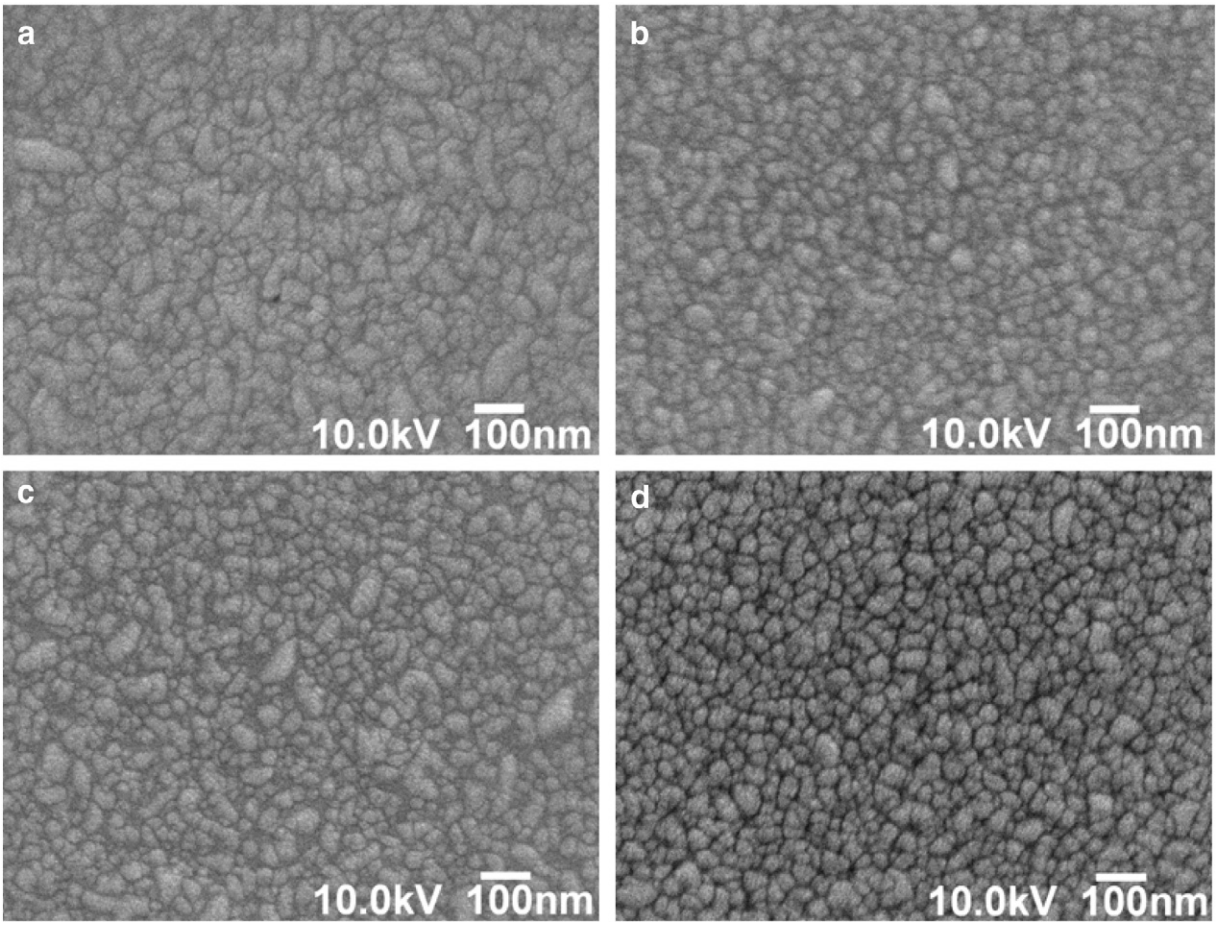

Fig. 4. SEM micrographs of AZO films grown on PET, at different sputtering pressures (a) 0.66, (b) 1.0, (c) 1.33 and (d) 2.0 Pa.

Resistivity decreases to a minimum value of 1.17 mΩ cm, for an Al buffer thickness of 10 nm. The decrease in resistivity may occur, because the elevated annealing temperature provides the atoms in the film with more energy, enhancing carrier concentrations, which may decrease the number of defects and improve the quality of the AZO films [22].

The quality of the AZO/Al/PET film was examined, for different thicknesses of Al buffer. The full widths at half maximum (FWHM) of (002) XRD, for as-deposited and annealed AZO/Al/PET, with Al buffer of different thicknesses, are shown in Table 4. The 2 nm thick Al buffer layer shows the smallest FWHM, for both as-deposited and annealed ZnO films. This result shows that the FWHM is decreased by annealing. However, for high transmittance, the thickness of the metal layer (Au, Ag and Al) may not exceed a certain threshold thickness. As the thickness of the metal layer increases, the transmittance decreases and reflection increases, as the film becomes a mirror [23]. Fig. 10 shows the optical transmittance for AZO films, for different thicknesses of Al buffer. It shows that the transmittance decreases, as the thickness of the Al buffer increases.

A cross-sectional view of the film is shown in Fig. 11. The films were very compact, homogeneous, exhibited perfect adherence to the PET substrate and were without defects or voids. The columns are vertical to the substrate, showing a growth with a marked *c*-axis orientation [24]. The detailed geometrical structure of the AZO films was also determined, using high-resolution transmission electron microscopy (HRTEM). Fig. 12 shows the TEM images of the AZO crystalline particles and the selected-area electron diffraction (SAED) pattern from the as-deposited sample. The SAD pattern is composed

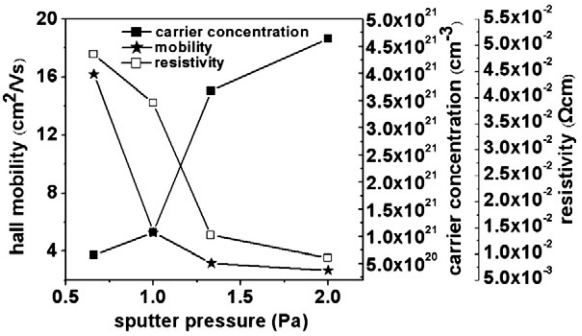

Fig. 5. The resistivity, Hall mobility and carrier concentrations for AZO thin films grown on PET, as a function of sputtering pressure.

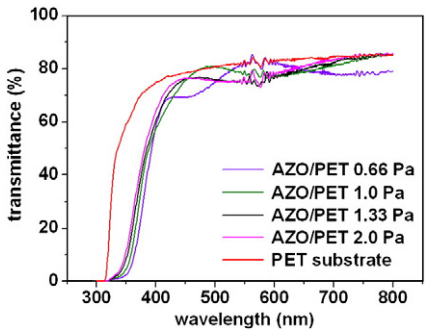

Fig. 6. Optical transmittance of AZO films deposited on PET, at different sputtering pressures.

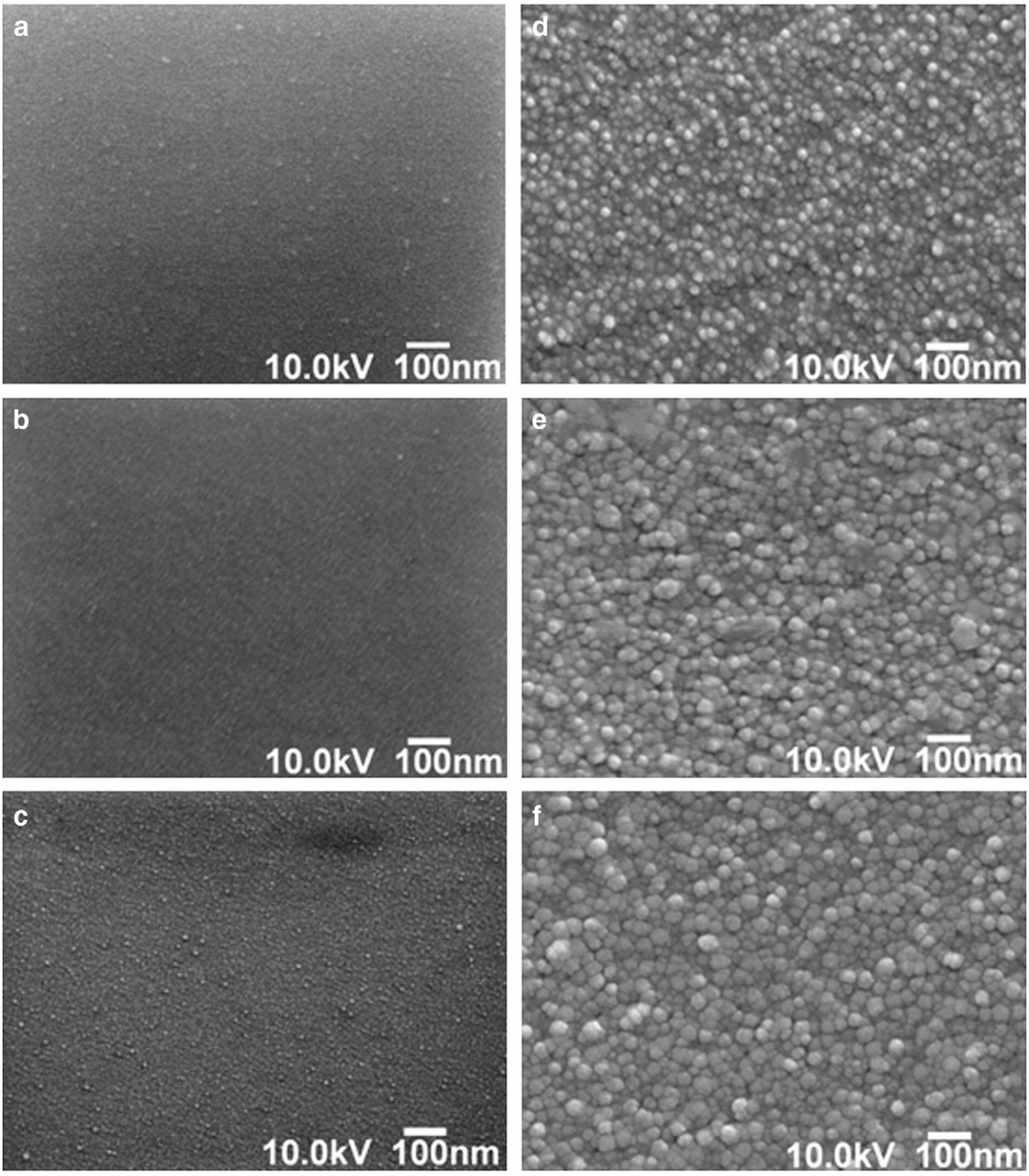

Fig. 7. SEM micrographs (a–c) Al buffer surfaces and (d–f) AZO films surfaces. (a) Al 2 nm/PET (d) AZO/Al 2 nm/PET. (b) Al 5 nm/PET (e) AZO/Al 5 nm/PET. (c) Al 10 nm/PET (f) AZO/Al 10 nm/PET.

of a series of rings, which provides further evidence that these column structures are indeed ZnO, with the (002) plane parallel to the substrate surface [4].

4. Conclusions

Using RF magnetron sputtering, at room temperature, this paper investigates the influence of argon gas pressure, in the sputtering process, on the structural, morphological and electrical properties of AZO films deposited on flexible PET substrates. The minimum values for Hall mobility and resistivity were 2.68 $cm^2/V\,s$ and 9.22 mΩ cm, respectively, for the film deposited at 2.0 Pa. For AZO films deposited on PET substrates, with and without an Al buffer layer, the peel-off stresses were 24.35 and 17.31 MPa, respectively. This demonstrates that the Al buffer layer increases the adhesive strength of the AZO thin films.

As the thickness of the Al buffer layer increases, the crystalline quality of the AZO films is improved and the grain sizes become larger and more uniformly distributed. However, visible range transmittance decreases, as thickness of the Al buffer increases. Annealing improves the crystalline and microstructure quality of the films. By annealing at 120 °C, in a vacuum, for a period of 30 min, the AZO/Al/PET films (for buffer thicknesses of 10 nm) show values for electrical resistivity of 1.17 mΩ cm and for carrier concentration of $2.68\times10^{22}\ cm^{-3}$.

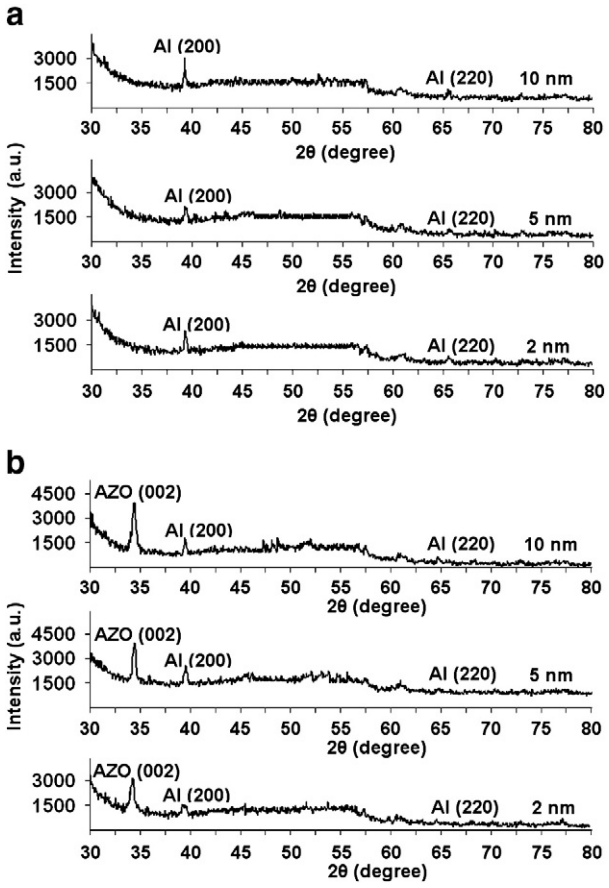

Fig. 8. X-ray diffraction spectra for (a) Al/PET and (b) AZO/Al/PET, for different thicknesses of Al buffer.

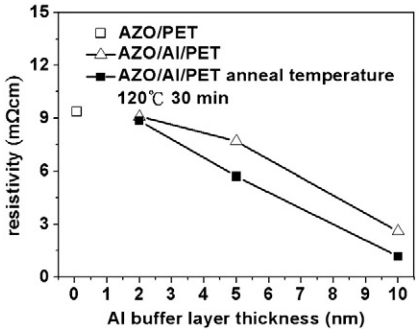

Fig. 9. The resistivity of AZO thin films grown on Al/PET, as a function of Al buffer thickness, for AZO films of thickness 200 nm, deposited using a sputter pressure of 2.0 Pa.

Table 4
The FWHM of the (002) diffraction peaks for AZO thin films grown on PET substrates, with Al buffer layers of different thicknesses.

Al buffer layer thickness (nm)	As-deposited or annealed	FWHM
0	As-deposited	0.352
0	Annealed	0.341
2	As-deposited	0.334
2	Annealed	0.329
5	As-deposited	0.373
5	Annealed	0.356
10	As-deposited	0.367
10	Annealed	0.341

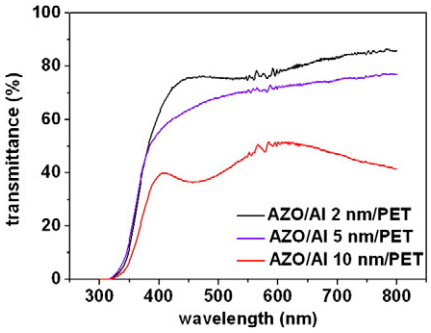

Fig. 10. Optical transmittance vs. wavelength, for AZO/Al/PET thin film with various thicknesses of Al buffer.

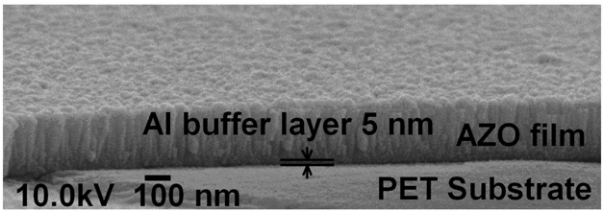

Fig. 11. Cross-sectional SEM images of AZO films grown on an Al buffer.

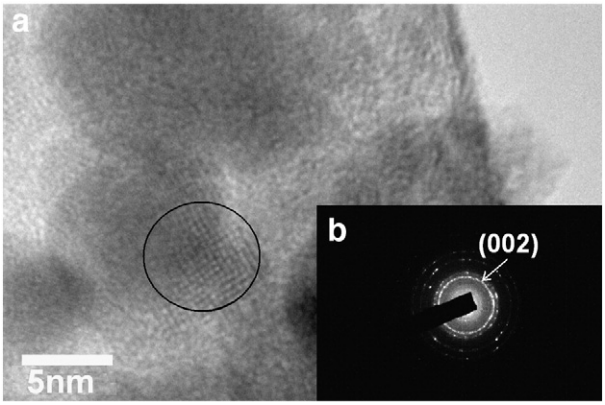

Fig. 12. TEM images and SAED pattern for as-deposited AZO films.

References

[1] B.D. Ahn, S.H. Oh, C.H. Lee, G.H. Kim, H.J. Kim, S.Y. Lee, J. Cryst. Growth 309 (2007) 128.
[2] Y.M. Hu, C.W. Lin, J.C.A. Huang, Thin Solid Films 497 (2006) 130.
[3] C.Y. Hsu, Y.C. Lin, L.M. Kao, Y.C. Lin, Mater. Chem. Phys. 124 (2010) 330.
[4] B. Houng, C.S. Hsi, B.Y. Hou, S.L. Fu, Vacuum 83 (2009) 534.
[5] H. Ko, W.P. Tai, K.C. Kim, S.H. Kim, S.J. Suh, Y.S. Kim, J. Cryst. Growth 277 (2005) 352.
[6] Y.M. Chung, C.S. Moon, M.J. Jung, J.G. Han, Surf. Coat. Technol. 200 (2005) 936.
[7] A. Miyake, T. Yamada, H. Makino, N. Yamamoto, T. Yamamoto, Thin Solid Films 517 (2009) 3130.
[8] A. Miyake, T. Yamada, H. Makino, N. Yamamoto, T. Yamamoto, Thin Solid Films 517 (2008) 1037.
[9] D.H. Zhang, T.L. Yang, J. Ma, Appl. Surf. Sci. 158 (2000) 43.
[10] C.Y. Hsu, T.F. Ko, Y.M. Huang, J. Eur. Ceram. Soc. 28 (2008) 3065.
[11] R.C. Hibbeler, Mechanics of Materials, Pearson/Prentice Hall, Singapore, ISBN: 0-13-124-571-6, 2003, p. 24.
[12] L. Zhai, G. Ling, J. Li, Y. Wang, Mater. Lett. 60 (2006) 3031.
[13] Q.B. Ma, Z.Z. Ye, H.P. He, L.P. Zhu, B.H. Zhao, Mater. Sci. Semicond. Process 10 (2007) 167.
[14] J. Lee, H. Jung, J. Lee, D. Lim, K. Yang, J. Yi, W.C. Song, Thin Solid Films 516 (2008) 1634.
[15] Q.B. Ma, Z.Z. Ye, H.P. He, S.H. Hu, J.R. Wang, L.P. Zhu, Y.Z. Zhang, B.H. Zhao, J. Cryst. Growth 304 (2007) 64.

[16] K. Jang, H. Park, S. Jung, N.V. Duy, Y. Kim, J. Cho, H. Choi, T. Kwon, W. Lee, D. Gong, S. Park, J. Yi, D. Kim, H. Kim, Thin Solid Films 518 (2010) 2808.
[17] Y. Zhang, H. Zheng, J. Su, B. Lin, Z. Fu, J. Lumines. 124 (2007) 252.
[18] J.Y. Tseng, Y.T. Chen, M.Y. Yang, C.Y. Wang, P.C. Li, W.C. Yu, Y.F. Hsu, S.F. Wang, Thin Solid Films 517 (2009) 6310.
[19] Z.L. Pei, X.B. Zhang, G.P. Zhang, J. Gong, C. Sun, R.F. Huang, L.S. Wen, Thin Solid Films 497 (2006) 20.
[20] E. Fortunato, A. Goncalves, V. Assuncao, A. Marques, H. Aguas, L. Pereira, I. Ferreira, R. Martins, Thin Solid Films 442 (2003) 121.
[21] D.R. Sahu, J.L. Huang, Thin Solid Films 516 (2007) 208.
[22] Z.B. Fang, Z.J. Yan, Y.S. Tan, X.Q. Liu, Y.Y. Wang, Appl. Surf. Sci. 241 (2005) 303.
[23] D.R. Sahu, J.L. Huang, Thin Solid Films 515 (2006) 876.
[24] Z. Ben Ayadi, L. El Mir, K. Djessas, S. Alaya, Thin Solid Films 517 (2009) 6305.